Journal of Japan Association for Earthquake Engineering, Vol. 22, No. 3, 2022

ESTIMATION OF THE EFFECT OF MATERIAL UNCERTAINTY ON SURFACE FAULT DISPLACEMENT USING LATIN HYPERCUBE SAMPLING

Kazumoto HABA[1], Akihito HATA[2], Masataka SAWADA[3] and Muneo HORI[4]

[1] Member, Dr. Sc., Nuclear Facilities Division, Taisei Corporation,
Tokyo, Japan, hb-kzm00@pub.taisei.co.jp
[2] Member, Dr. Eng., Technology Center, Taisei Corporation,
Tokyo, Japan, hata@ce.taisei.co.jp
[3] Dr. Eng., Nuclear Risk Research Center, Central Research Institute of Electric Power Industry,
Chiba, Japan, sawada@criepi.denken.or.jp
[4] Member, Ph.D., Japan Agency for Marine-Earth Science and Technology,
Chiba, Japan, horimune@jamstec.go.jp

ABSTRACT: Reliable estimation of surface fault displacements is necessary for the safety of infrastructure and buildings. It is essential to consider various uncertainties in the fault rupture process for the reliable estimation. In this study, the effect of material uncertainties on surface fault analysis was examined by performing ensemble simulations using Latin hypercube sampling. The convergence of probabilistic responses versus the number of samples was analyzed by computing multiple sample sets. It is shown that the critical value of the primary fault base slip at which surface faults appear on the ground are strongly affected by material uncertainties. The probabilistic distribution of the critical base slip can be approximated well by the log-normal distribution when the material properties are assumed to be log-normal random variables. The mean and standard deviation can be estimated with errors of several centimeters by conducting ten simulations when the material properties have coefficients of variance of less than 0.3.

Keywords: *Surface fault displacement, High performance computing, Material uncertainty, Latin hypercube sampling, Nuclear power plant*

1. INTRODUCTION

Surface fault displacement can cause extensive damage to infrastructure and buildings, although it is a rare event. Infrastructures actually suffered damage from surface faults caused by earthquakes in Taiwan and Turkey in 1999. It is pointed out that assessment of fault displacement is essential to ensure the safety of nuclear power plants (NPPs)[1)]. Regulation standards for NPPs in Japan requires that “facilities with important safety functions shall be established on the ground that has been confirmed to have no outcrop of a fault, etc. with the possibility of becoming active in the future”[2)]. NPPs are built at a location

distant from the primary fault based on a detailed geological survey. Therefore, it is important to estimate the occurrence of secondary fault displacement accompanying a primary fault activity to ensure the safety of NPPs.

Numerical simulations based on continuum mechanics are one of the prediction methods for secondary fault activity. However, three-dimensional (3D) simulation of the fault rupture is difficult because the scale of a 3D geological analytical model becomes large. We developed a high-performance computing finite element method (HPC-FEM) for surface fault analysis[3)–5)]. Here, E-FrontISTR was used in the simulation as a platform for the HPC-FEM. E-FrontISTR was developed based on FrontISTR[6)], an open-source large-scale parallel FEM program, by Taisei Corporation, Central Research Institute of Electric Power Industry, The University of Tokyo, Tokyo Electric Power Services CO., National Research Institute for Earth Science and Disaster Resilience, and Ark Information Systems. The following two-step simulation is reasonable for the assessment of secondary fault activity[1)]: (1) evaluating the crustal deformation caused by the primary fault slip that is based on the elastic theory of dislocations[7)]; and (2) evaluating the displacement and deformation of the target area around the NPPs by analyzing a 3D high-fidelity model with HPC-FEM, where the displacement calculated in step (1) is applied to the boundary of the target area. Assessment of secondary fault activity requires the estimation of the critical scale of earthquakes in which surface faults appear on the ground. In surface fault analysis, it is important to evaluate the critical value of the primary fault base slip, denoted by Δ_c, because the value of the primary fault slip is associated with the seismic moment. Thus far, we conducted an analysis against the 2014 Nagano-ken-hokubu earthquake in Japan and showed that the estimated surface slips were in good agreement with the observed surface slips[8)].

For a more reliable estimation, it is essential to consider uncertainties in the fault rupture process because there are certain limitations regarding the quality and quantity of available data of underground structures, source fault dynamics, material properties, etc. To consider uncertainties in underground structures and source fault dynamics, simulations must be conducted with numerous scenarios. However, ensemble computing is applicable for continuous variables with probability density functions, such as material uncertainties. Thus far, we have utilized ensemble computing using a simple rectangular analytical model to evaluate the variability in surface faults induced by material uncertainties[9)]. In that study, uncertainties in Young's modulus of the rock mass and the friction angle on the fault planes were considered with the sample points obtained by orthogonal sampling in which the sampling points were set systematically at regular intervals. This study indicates that Δ_c is smaller when the Young's modulus is larger and the friction angle is smaller, and Δ_c has a unimodal distribution, which can be assumed by a log-normal distribution. However, the orthogonal sampling causes an increase in the number of samples because the number of samples is proportional to the power of the number of independent uncertain material properties.

In this study, we evaluated the effects of material uncertainties on surface faults with ensemble computing using Latin hypercube sampling (LHS)[10)]. In particular, attention was given to the Δ_c at the evaluation points and the probabilistic responses and the convergence of the second-order moment against the number of samples.

The remainder of this paper is organized as follows. Section 2 explains the procedure of surface fault analysis and LHS. Section 3 presents the basic behavior of simulations based on the analysis using the mean value of material properties. The probabilistic response is presented in Section 4. Finally, this paper is summarized in Section 5.

2. ANALYTICAL METHOD AND CONDITION

2.1 Method of surface fault Analysis

In this study, we conducted a surface fault analysis for the 2014 Nagano-ken-hokubu Earthquake[11)], which is a reverse-type earthquake with a compression axis in the west–northwest and east–southeast directions. As shown in Fig. 1, a 9-km-long surface rupture was observed on the Kamishiro Fault, which

was recognized and mapped on the Japanese fault map. Additionally, secondary faults, named secondary faults E, N, and S, were observed[11), 12)]. The maximum net slip values on the primary fault and secondary faults were approximately 1.0 m and 0.5 m, respectively[12)].

Figure 2 (a) shows an analytical model of the target region, which had an area of 5 km × 5 km and a depth of 1 km around the northern end of the surface rupture. The J-SHIS database[13)] of the national research institute for earth science and disaster resilience was used to determine the two geological layers of the region. Figure 2 (b) shows the fault plans in the model corresponding to the primary fault and three secondary faults. The strike, dip, and location of the fault planes were determined based on the observation, as shown in Table 1. In Fig. 2 (b), planes AA'D' D and BB'C' C are the primary fault plane and secondary fault E plane, respectively. O_P and O_S in Fig. 2 (b) are the evaluation points on the ground surface positioned at the center of the analytical model. Second-order tetrahedral solid elements and triangular joint elements were used to construct the ground and fault planes, respectively. Each triangular element had a size of approximately 50 m, resulting in 2,174,601 DOFs.

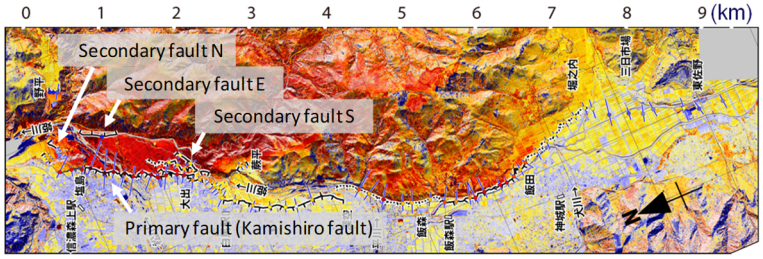

Fig. 1 Distribution of surface fault based on a differential analysis of multi LiDAR-DEM data[12)]

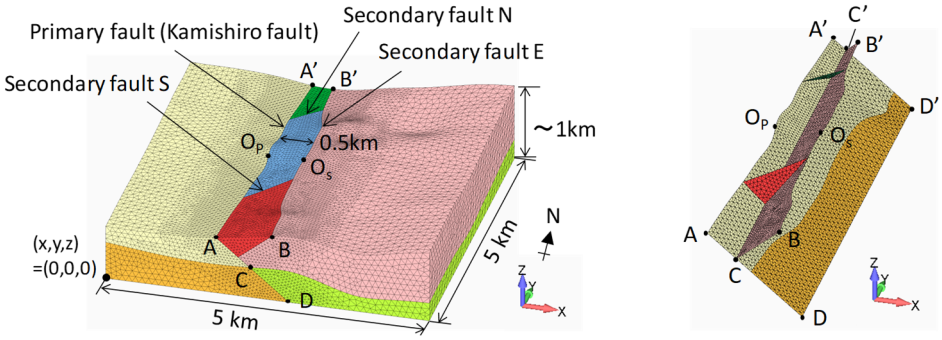

(a) Overall view (b) Fault planes

Fig. 2 Analytical model. It has two geological layers and four fault planes that are indicated by boundaries of colored blocks.

Table 1 Configuration of fault planes in an analytical model

Fault	Strike	Dip	Position relative to primary fault
Primary fault (Kamishiro fault)	North–northeast (+y direction)	40°	-
Secondary fault E	South–Southwest	40°	0.5 km east from primary fault
Secondary fault N	East–northeast	40°	Connected to primary fault at y = 3.85 km and the surface of the ground
Secondary fault S	West–southwest	40°	Connected to primary fault at y = 1.35 km and the surface of the ground

We applied a simple slip law to fault planes, which was modeled considering the mathematical instability of the solution[15)], as shown in Fig. 3. The shear spring constant k and displacement gap u of the nonlinear spring are related as follows:

$$k = \begin{cases} k_0 - \frac{k_0 - k_d}{u_{\mathrm{cr}}} u & (u \le u_{\mathrm{cr}}) \\ k_d & (u_{\mathrm{cr}} \le u) \end{cases}, \tag{1}$$

where k_0 and k_d are the initial and final values of the shear stiffness, respectively, and u_{cr} is the critical slip at which the shear stiffness changes. The slip-traction relationship (refer to Fig. 3 (b)) has a peak strength $\tau_{\max}$. The slip u rapidly increases when the external force becomes larger than $\tau_{\max}$. After slipping, the traction decreases with an increase of slip u as with the linear slip-weakening friction law[16] which used rapture analysis for deep fault plane. However, the traction gradually recovers with the small shear stiffness k_d when u exceeds u_{cr}, that prevents the lack of solution. $\tau_{\max}$ was determined by Coulomb's friction law, $\tau_{\max} = \sigma_n \tan\phi + c$, where σ_n, c, and ϕ are the normal stress, cohesion, and friction angle, respectively.

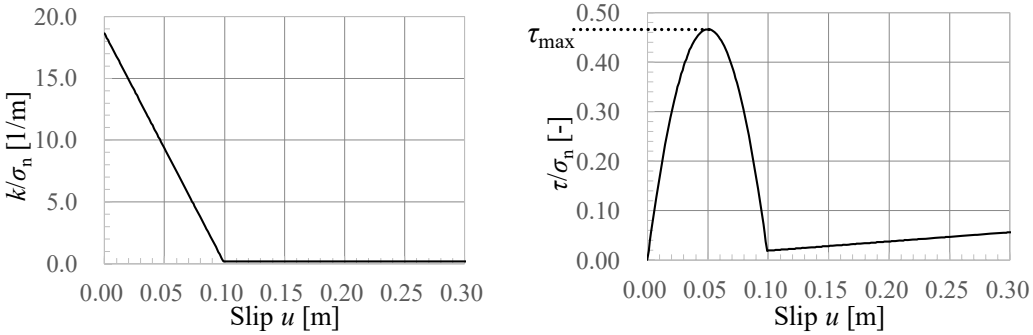

(a) Slip–spring coefficient relationship (b) Slip–traction relationship

Fig. 3 Constitutive law for fault plane. Here $u_{\mathrm{cr}} =$ 0.1 m.

Table 2 shows the mean value and coefficient of variation (COV) of material properties, in which the mean value is the same as the one used by Sawada et al (2018)[8]. Here, the material properties of the rock mass are determined based on the J-SHIS database[13]. The cohesion and friction angle of the fault plane are determined by reference to the experimental value of the crushed zone in nuclear sites[8]. In this study, we assumed that Young's modulus of the ground layers and the friction angle on the fault planes follow an independent log-normal distribution with COV = 0.3 and 0.15, respectively. These settings are consistent with ones used in a standard for procedure of seismic probabilistic risk assessment for nuclear power plants[14] of atomic energy society of Japan, in which it was suggested that a material property can be assumed to be a log-normal distribution when an appropriate database is not available.

Table 2 Material properties

	Material property [unit]	Mean	COV
Rock of the first layer	Young's modulus E_1 [GPa]	10.03	0.30
	Poisson's ratio ν_1 [-]	0.3491	-
	Density ρ_1 [ton/m^3]	2.200	-
Rock of the second layer	Young's modulus E_2 [GPa]	27.73	0.30
	Poisson's ratio ν_2 [-]	0.3097	-
	Density ρ_2 [ton/m^3]	2.400	-
Fault plane	Friction angle ϕ [deg]	25.0	0.15
	Cohesion c [MPa]	0.025	-
	Ratio of dynamic to quasi-static shear modulus k_d/k_0 [-]	0.01	-
	Critical slip u_{cr} [m]	0.1	-

Surface fault analysis is conducted by quasi-static analysis taking over the result of normal stress on fault planes estimated by self-weight analysis. The displacement boundary condition is determined by conventional dislocation theory[7]. It was pointed out that the forced displacement on the boundary of an analytical model can constraint a slip of secondary faults that reaches the boundary[17]. However, the condition in this study does not fall under that situation. Geological structure and secondary fault planes can be considered in FEM analysis although the ground is assumed to be a homogenous semi-infinite elastic body in the elastic dislocation theory. The slip distribution across the Kamishiro fault, which becomes the initial condition of the elastic dislocation theory, was set based on the result of source inversion obtained from the geospatial information authority of Japan[18]. However, the slip distribution wherein a superficial part shallower than E.L. −3 km is corrected by the observed surface slip as the study of Sawada (2018)[8]. Calculation of the elastic dislocation theory is conducted with Coulomb 3.3[19]. We set the maximum value of the primary slip to 4.0 m. The displacement obtained by the elastic dislocation theory is incrementally loaded to the bottom boundary of the analytical model in 200 steps.

2.2 LHS for probabilistic analysis

In this study, the effects of material uncertainties in surface fault analysis were assessed through simulations using LHS. LHS is a method of experimental design and sampling[10], which can be assess probabilistic response with a relatively small number of sample points. Figure 4 shows an overview of LHS, in which two independent probabilistic variables $X_1(\omega)$ and $X_2(\omega)$ are considered. In LHS, the sample space of each probabilistic variable is divided into n equally probable subspaces, and a sample is chosen from each subspace. Thereafter, n sample sets were obtained as a random combination of samples of each probabilistic variable. When each range of m probabilistic variables is divided into n intervals, the number of samples is n in LHS, although it is n^m in the orthogonal method.

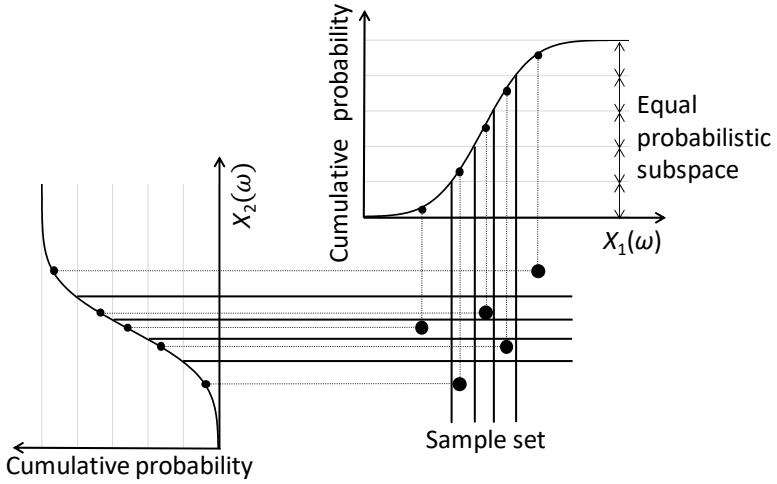

Fig. 4 Overview of LHS. Probabilistic range of each variable, $X_1(\omega)$ and $X_2(\omega)$, is divided into 5 ranges.

In this study, to confirm the convergence between the probabilistic result and the number of samples, we conducted analyses with multiple sample sets having different numbers of samples. Probabilistic results are variable in the same number of samples caused by randomness of creation of samples. Focusing on moment characterizing probabilistic response, lower-order ones such as mean and variance can be estimated with a small error using a relatively small number of samples. From the point of actual practice, it is important to confirm the number of samples which make it possible to evaluate the moment of random variables with high accuracy. Table 3 lists the sample sets used. We used 14 sample sets in which the maximum number of samples was 120. Note that Set20-3, Set40-2, Set60-2, Set80, and Set120 were obtained as a combination of more than a sample set.

Table 3 Sample set

No.	ID.	Number of samples	Component sample set
1	Set10-1	10	
2	Set10-2	10	
3	Set10-3	10	
4	Set20-1	20	
5	Set20-2	20	
6	Set20-3	20	Set10-1, Set10-2
7	Set30-1	30	
8	Set30-2	30	
9	Set40-1	40	
10	Set40-2	40	Set10-1, Set10-2, set20-2
11	Set60-1	60	
12	Set60-2	60	Set30-1, set30-2
13	Set80	80	Set10-1, Set10-2, set20-2, Set40-1
14	Set120	120	Set30-1, set30-2, set60-1
Total number of samples		230	

We illustrate a way to create a sample set from two sample sets. Figure 5 shows an overview of how to create a sample set with six samples from two sample sets with three samples. First, a sample set with three samples is produced in STEP 1. Next, in STEP 2, the sample space is divided into six equally probable subspaces and the samples are allocated in the subspaces. In that case, 3 times 3 subspaces become blank. Finally, newly produced three samples are mapped in the 3 times 3 blank subspaces in STEP 3. In this study, using a similar process, Set20-3, Set40-2, Set60-2, Set80, and Set120 are produced. The components sample set is shown in table 3. In this study, we conduct 230 calculations using 230 independent samples. Figure 6 describes Young's modulus of the ground layers and the friction angle on the fault planes obtained from each sample. Note that there is no overlap in the 230 samples.

Furthermore, we conducted a sensitivity analysis using the material properties of mean $\pm 1\sigma$, as shown in Table 4, to examine the effect of each material property. Here, Young's moduli of the two layers are perfectly correlated.

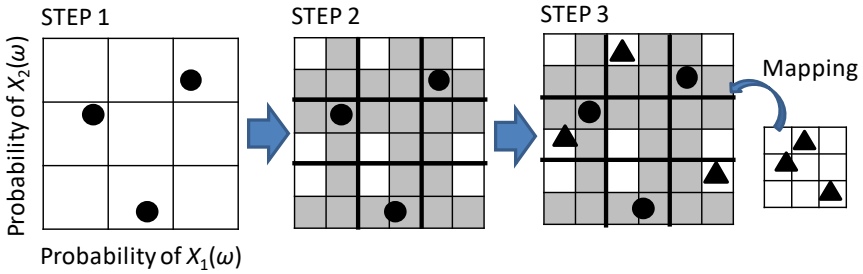

Fig. 5 Overview of how to produce a new sample set from two sample sets. Here, $X_1(\omega)$ and $X_2(\omega)$ are random variables, probabilistic range of each variable is divided into 3 or 6 ranges.

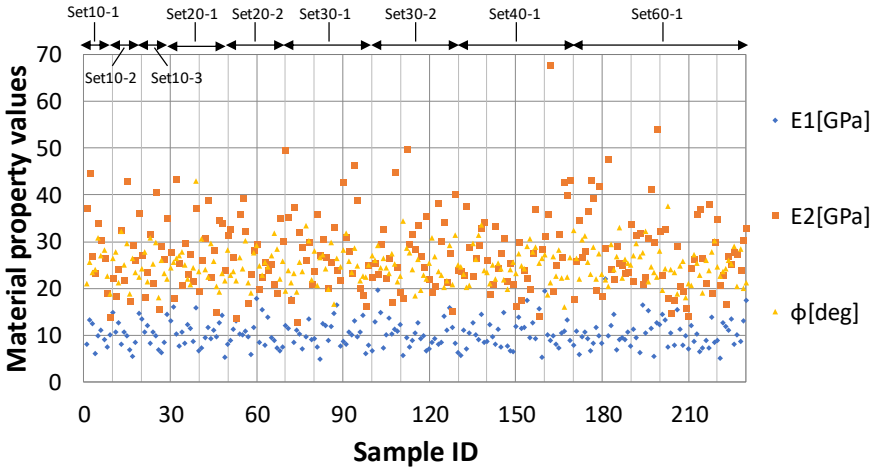

Fig. 6 Material properties of all samples

Table 4 Material properties for sensitivity analysis. Here material properties except for Young's modulus and the friction angle are described in Table 2.

Case ID	Young's modulus of rock		Friction angle of fault plane
	E_1 [GPa]	E_2 [GPa]	ϕ [deg]
Mean	10.03	27.73	25.00
Mean±1σ (E)	10.03±3.01	27.73±8.32	25.00
Mean±1σ (ϕ)	10.03	27.73	25.00±3.75

3. TYPICAL BEHAVIOR OF FAULT DISPLACEMENT

In this section, we show the typical response of surface fault analysis based on the simulation using the mean value of the material properties in Table 2. Figures 7 and 8 show the computed slip distributions on the primary and secondary fault E, respectively. Here, Fig. 7 (a), (b), (c), and (d) are the result at the maximum input base slip Δ = 0.4, 0.8, 1.8, and 2.8 m, and Fig. 8 (a) and (b) are ones at Δ = 1.8 m and 2.8 m, respectively. Figure 7 illustrates that the input base slip propagates and disperses on the primary fault, and the slip reaches the ground surface. The surface slip of secondary fault E also appears at Δ = 2.8 m. When a surface secondary fault appears, the slip of the region of the primary fault near the secondary fault becomes small because the occurrence of a surface fault causes stress release of the rock mass near the fault plane. This analysis succeeded in reproducing the movement of the secondary faults.

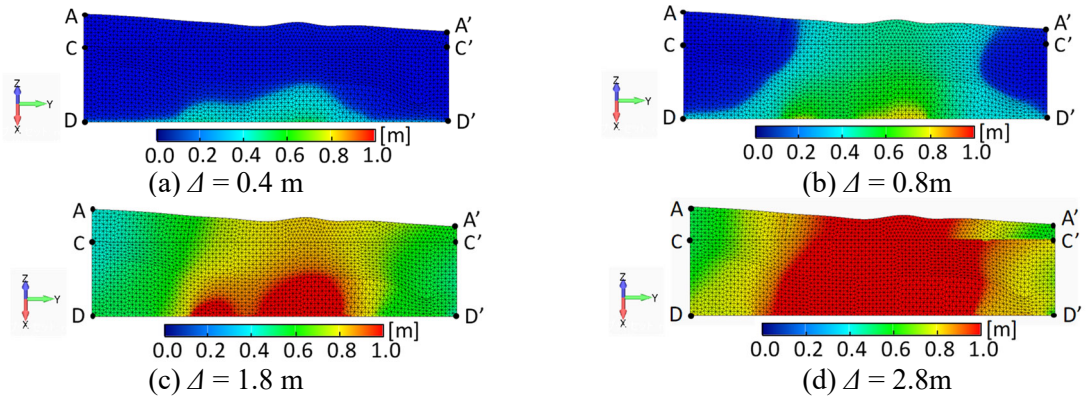

Fig. 7 Distribution of slip on the primary fault plane at an input slip of 0.4, 0.8, 1.8 m and 2.8 m

(a) Δ = 1.8 m (b) Δ = 2.8m

Fig. 8 Distribution of slip on secondary fault E plane at an input slip of 1.8 m and 2.8 m

Figure 9 shows the relationship between Δ and surface slip at the evaluation points O_P and O_S of the primary and secondary faults E, as shown in Fig. 2 (b). A surface fault appears on the ground surface when Δ exceeds the critical value of the primary fault base slip, denoted by Δ_c. Here, Δ_c is defined as Δ when the surface fault slip becomes the critical slip u_{cr} in a precise sense. The Δ_c of the primary fault and secondary fault E are 0.70 m and 2.74 m, respectively. The surface slip on the primary fault and secondary fault E are approximately 1.1 m and 0.5 m, respectively, when the secondary surface fault slip appears, which agrees with the experimental data. Please refer to the paper of Sawada et al. (2018)[8] for details.

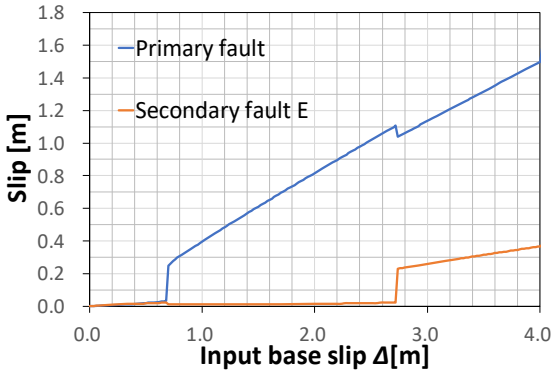

Fig. 9 Relationship between maximum input slip and surface slip at the evaluation points

4. ASSESSMENT OF EFFECT OF MATERIAL UNCERTAINTIES

4.1 Effect of each material property presented by sensitivity analysis

The effect of the Young's modulus of the rock mass and the friction angle of the fault plane was examined by sensitivity analysis. Figure 10 shows the relationship between Δ and surface slip at the evaluation points O_P and O_S in the sensitivity analysis. In Fig. 10, the solid line is the result of an analysis with material properties of mean value, the orange dashed line and dotted line are the results of the case with Young's modulus of mean $\pm 1\sigma$, respectively, and the green dashed line and dotted line are the results of the case with a friction angle of mean $\pm 1\sigma$, respectively. Figure 10 reveals that Δ_c decreases when Young's modulus becomes larger or the friction angle becomes smaller. These trends are in agreement with the results of Haba et al. (2018)[9].

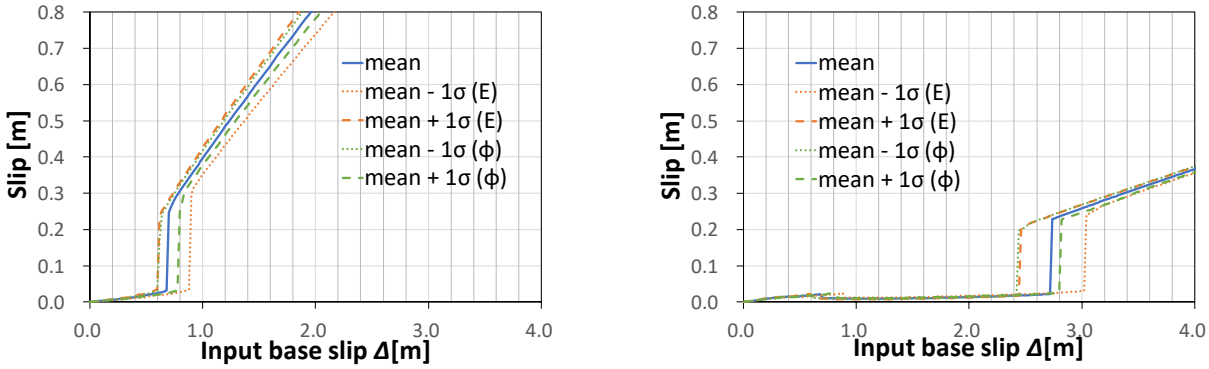

(a) Primary fault (b) Secondary fault E

Fig. 10 Relationship between maximum input slip and surface slip at the evaluation points obtained by sensitivity analysis

4.2 Probabilistic response of critical base slip with LHS

The probabilistic response of Δ_c was examined based on analyses using LHS. Figure 11 shows the relationship between Δ and surface slip at the evaluation points O_P and O_S for Set60-1. Figure 11 reveals that Δ_c of the primary fault and secondary fault E have considerable variability, in which the variability of the secondary fault is greater than that of the primary fault. Figure 12 illustrates a histogram of Δ_c for Set60-1. The green line in Fig. 12 is the approximated log-normal distribution, which is obtained by non-linear fitting of the mean and standard deviation using cumulative probability as the model function. Figure 13 shows the result of the fitting of the cumulative probability, which has an adjusted coefficient of determination[20] R^2 of 0.996. These results show that Δ_c of the primary fault and secondary fault E has a heavy right-tailed unimodal distribution, which can be assumed by a log-normal distribution. As a result, the second-order moment, that is the mean and standard deviation, provides a good indication of the probabilistic response of Δ_c.

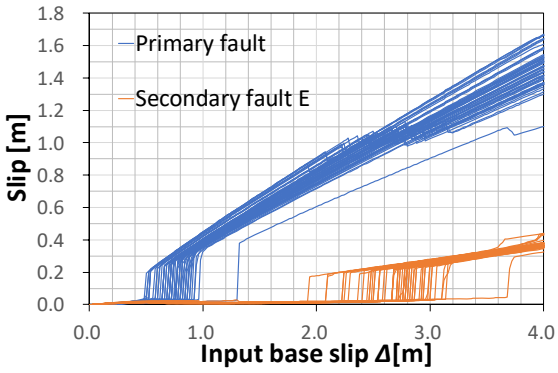

Fig. 11 Relationship between maximum input slip and surface slip at the evaluation points in the case of Set60-1

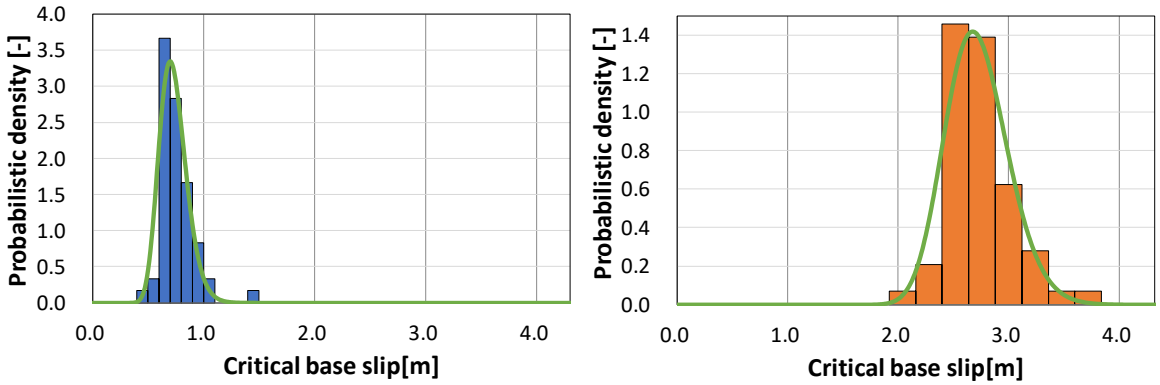

(a) Primary fault (b) Secondary fault E

Fig. 12 Histogram of Δ_c in the case of Set60-1, in which the green line denotes the fitted log-normal distribution.

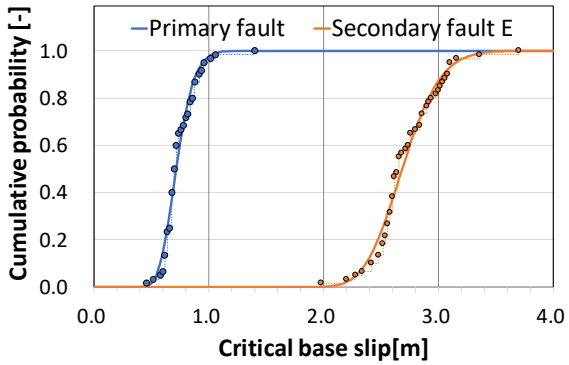

Fig. 13 Fitting of cumulative probability of Δ_c in the case of Set60-1.

Table 5 and Fig. 14 show the mean, standard deviation, and COV of Δ_c in all cases, in which the mean and standard deviation are obtained by fitting to a log-normal distribution. The deterministic results are shown in Fig. 14 for reference. The results of standard deviation suggest that material uncertainties more strongly affect Δ_c of secondary faults than one of the primary faults. Here, although the COV of the primary fault is larger than that of the secondary fault, the standard deviation can be more important in terms of the assessment of the occurrence of the surface fault and disaster defense.

We analyzed the convergence of the second-order moment with respect to the number of samples. In this study, error of the moment in the case of a sample set is defined as the difference between the result of the sample set and one obtained with all 230 samples, which can be viewed as a sample set of the Monte Carlo method. We judge that the variable converges when the error becomes less than 0.02 m because the minimum increment of the input base slip is 0.02 m.

Figure 15 shows the relationship between the number of samples and error in the mean and the standard deviation of Δ_c of the primary fault and secondary fault E. Figure 15 demonstrates that the error decreases according to an increase in the number of samples. In both the primary fault and secondary fault E, the error becomes less than 0.02 m with 60 samples and the mean and standard deviation converged. The error of mean and standard deviation of secondary fault E is 0.072 m and 0.029 m with 10 samples, respectively. From the point of actual practice, they can be estimated with high accuracy using a sample set of 10 samples obtained by LHS. To consider uncertainties in underground structures and source fault dynamics, we must conduct simulations with numerous scenarios. Therefore, we should examine the effect of material uncertainties with a minimum number of samples in each scenario. This study suggested that the effect of material uncertainties to Δ_c is predictable with several 10 samples of LHS.

Table 5 Mean and standard deviation of the critical base slip Δ_c

Sample ID	Primary fault			Secondary fault E		
	MEAN (m)	STD (m)	COV	MEAN (m)	STD (m)	COV
Deterministic	0.700	-	-	2.74	-	-
Set10-1	0.716	0.092	0.129	2.64	0.245	0.093
Set10-2	0.728	0.143	0.196	2.71	0.241	0.089
Set10-3	0.733	0.120	0.163	2.70	0.296	0.109
Set20-1	0.737	0.131	0.177	2.72	0.274	0.101
Set20-2	0.727	0.090	0.124	2.70	0.296	0.109
Set30-1	0.739	0.118	0.159	2.72	0.265	0.098
Set30-2	0.737	0.145	0.197	2.70	0.304	0.112
Set40-1	0.726	0.121	0.167	2.71	0.249	0.092
Set40-2	0.720	0.123	0.170	2.68	0.267	0.100
Set60-1	0.747	0.127	0.170	2.70	0.264	0.098
Set60-2	0.729	0.124	0.169	2.70	0.264	0.098
Set80	0.739	0.132	0.179	2.72	0.282	0.104
Set120	0.738	0.127	0.172	2.71	0.260	0.096

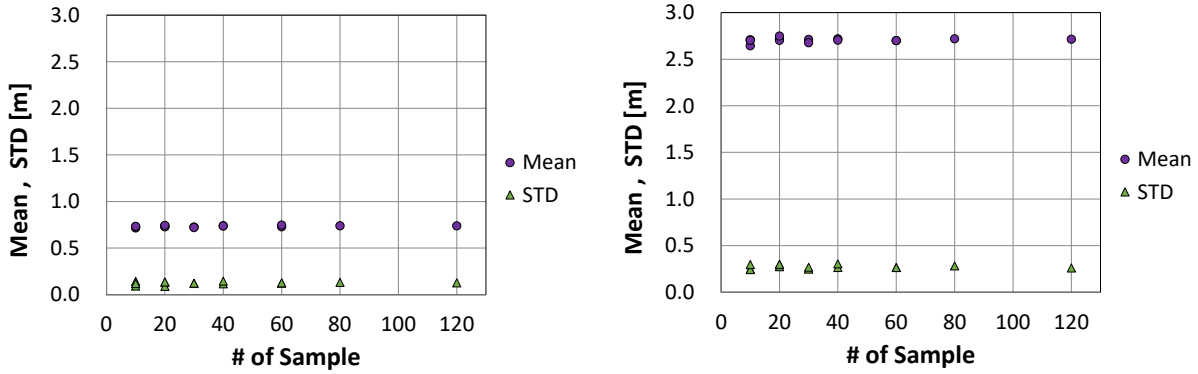

(a) Primary fault (b) Secondary fault E

Fig. 14 Relationship between second-order moment of the critical base slip Δ_c and the number of samples

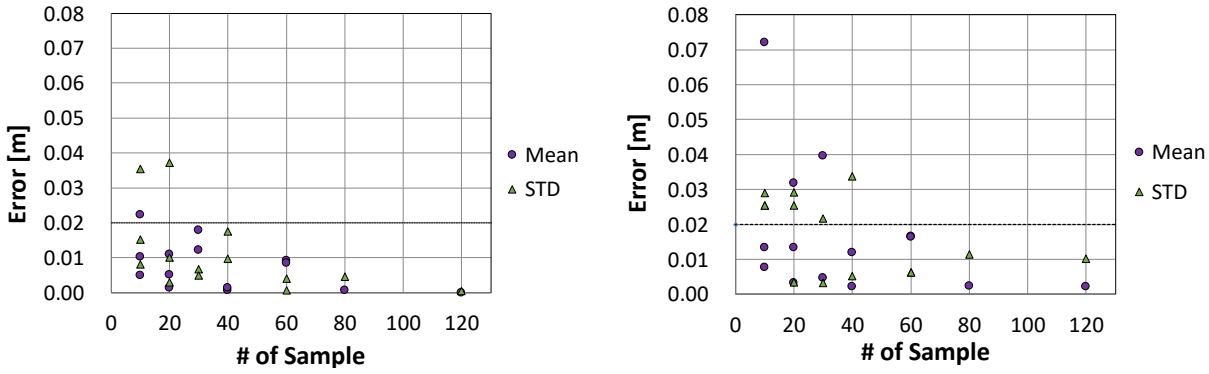

(a) Primary fault (b) Secondary fault E

Fig. 15 Relationship between the error of second-order moment of the critical base slip Δ_c and the number of samples, in which the error is the difference to the solution obtained with all 230 samples

5. CONCLUSIONS

In this study, we assessed the effect of material uncertainties on surface fault analysis using Latin hypercube sampling. The critical value of the primary fault base slip generating surface fault slip was precisely examined. As a result, it was found that material uncertainties more strongly affect the critical base slip of secondary faults than those of primary faults. The mean and standard deviation provide one of the best indications of the probabilistic response of the critical base slip because it has a heavy right-tailed unimodal distribution which can be assumed by a log-normal distribution. The mean and standard deviation are judged to converge with the 60 samples and can be estimated within an error of several centimeters in the case of 10 samples. The effect of material uncertainties should be examined with a minimum number of samples in each scenario because numerous scenarios must be considered to assess the uncertainties in underground structures and source fault dynamics.

Our future studies will focus on probabilistic surface fault analysis with numerous scenarios considering uncertainties in underground structures and source fault dynamics. Furthermore, we will examine the effect of the spatial correlation of material properties.

ACKNOWLEDGEMENT

This study was supported by commissioned projects from the Agency for Natural Resources and Energy, Ministry of Economy, Trade, and Industry, Japan.

REFERENCES

1) Japan Nuclear Safety Institute: Assessment Methods for Nuclear Power Plant against Fault Displacement, 50 pp., 2013.
2) Nuclear Regulation Authority: New Regulatory Requirements for Commercial Nuclear Power Reactors, 2013. https://www.nsr.go.jp/english/regulatory/ (last accessed on March 31, 2018).
3) Sawada, M., Haba, K. and Hori, M.: Computational Study on a Numerical Method for Fault Displacement Estimation, *Journal of Japan Society of Civil Engineers A2*, Vol. 72, No. 2, pp. I_675–I_685, 2016 (in Japanese).
4) Sawada, M., Haba, K. and Hori, M.: High Performance Computing for Fault Displacement Simulation, *Journal of Japan Society of Civil Engineers A2*, Vol. 73, No. 2, pp. I_699–I_710, 2017 (in Japanese).
5) Sawada, M., Haba, K. and Hori, M.: Estimation of Surface Fault Displacement by High Performance Computing, *Journal of Earthquake and Tsunami*, Vol. 12, No. 4, 1841003, 2018.
6) FrontISTR Consortium, FrontISTR, https://www.frontistr.com/, (last accessed on February 1, 2022) (in Japanese).
7) Okada, Y.: Surface Deformation Due to Shear and Tensile Faults in a Half-Space, *Bulletin of the Seismological Society of America*, Vol. 75, No. 4, 1135–1154, 1985.
8) Sawada, M., Haba, K. and Hori, M.: Evaluation of Fault Displacement in a Real Earthquake with Faulting by High Performance Computing, *Journal of Japan Society of Civil Engineers A2*, Vol. 74, No. 2, pp. I_627–I_638, 2018 (in Japanese).
9) Haba, K. Sawada, M. and Hori, M.: Application of High Performance Computing to Probabilistic Fault Displacement Simulation with Uncertainties of Fault and Soil Properties, *Journal of Japan Society of Civil Engineers A2*, Vol. 74, No. 2, pp. I_683–I_692, 2018 (in Japanese).
10) Schuëller, G. I., Bucher, C. G., Bourgund, U. and Ouypornprasert, W.: On Efficient Computational Schemes to Calculate Structural Failure Probabilities, *Probabilistic Engineering Mechanics*, Vol. 4, No. 1, 10–18, 1989.
11) Ishimura, D., Okada, S., Niwa, Y. and Toda, S.: The Surface Rupture of the 22 November 2014 Nagano-Ken-Hokubu Earthquake (Mw 6.2), along the Kamishiro Fault, Japan, *Active Fault Research*, No. 43, pp. 95–108, 2015 (in Japanese).
12) Aoyagi, Y.: Fault Displacement Distribution of the 2014 Nagano-Ken Hokubu Earthquake Based

on a Differential Analysis of Multi LiDAR-DEM Data, *2016 Japan Geoscience Union*, SSS31-18, 2016.
13) National Research Institute for Earth Science and Disaster Resilience: Japan Seismic Hazard Information Station, https://www.j-shis.bosai.go.jp/en/, (last accessed on March 31, 2018).
14) Atomic Energy Society of Japan: A Standard for Procedure of Seismic Probabilistic Risk Assessment for Nuclear Power Plants, 267 pp., 2015.
15) Haba, K. Sawada, M. and Hori, M.: On Fundamental Mechanism and Mathematical Instability of Fault Displacement, *Journal of Japan Society of Civil Engineers A2*, Vol. 75, No. 1, pp. I 55–I 67, 2019 (in Japanese).
16) Ida, Y.: Cohesive Force across the Tip of a Longitudinal-Shear Crack and Griffith's Specific Surface Energy, *Journal of Geophysical Research*, Vol. 77, pp. 3796–3805,1972.
17) Haba, K. Sawada, M. and Hori, M.: Study on Application of High Performance Computing to Fault Displacement Simulation, *Journal of Japan Society of Civil Engineers A2*, Vol. 72, No. 2, pp. I_821–I_830, 2017 (in Japanese).
18) Geospatial Information Authority of Japan: https://www.gsi.go.jp/common/000188709.pdf, 2015 (last accessed on March 31, 2018) (in Japanese).
19) Toda, S., Stein, R. S., Sevilgen, V. and Lin, J.: Coulomb3.3 Graphic-Rich Deformation and Stress-Change Software for Earthquake, Tectonic, and Volcano Research and Teaching User Guide, U.S. Geological Survey, Open-File Report 20111060, 63 pp., 2011.
20) Theil, H.: *Economic Forecasts and Policy*, North-Holland Publishing Company, Amsterdam, The Netherland, 567 pp., 1961.

(Original Japanese Paper Published: January, 2020)
(English Version Submitted: February 01, 2022)
(English Version Accepted: March 09, 2022)